Translational Oncology 21 (2022) 101371

Contents lists available at ScienceDirect

Translational Oncology

journal homepage: www.elsevier.com/locate/tranon

Original Research

Long non-coding RNA ZNF667-AS1 retards the development of esophageal squamous cell carcinoma via modulation of microRNA-1290-mediated PRUNE2

Ying-Juan Zheng [a], Tian-Song Liang [b], Juan Wang [b], Jing-Yi Zhao [b], Su-Nan Zhai [b], Dao-Ke Yang [a,b,*], Li-Dong Wang [a,*]

[a] State Key Laboratory of Esophageal Cancer Prevention & Treatment, The First Affiliated Hospital of Zhengzhou University, Zhengzhou 450052, PR China
[b] Department of Radiotherapy, The First Affiliated Hospital of Zhengzhou University, Zhengzhou 450052, PR China

ARTICLE INFO

Keywords:
Esophageal squamous cell carcinoma
Long non-coding RNA ZNF667-AS1
microRNA-1290, PRUNE2
Proliferation
Migration
Invasion

ABSTRACT

Abnormal long non-coding RNAs (lncRNAs) have been detected in esophageal squamous cell carcinoma (ESCC). Here, we focused on lncRNA ZNF667-AS1 and its downstream mechanism in ESCC progression. Differentially expressed lncRNAs in ESCC were predicted by bioinformatics analysis. ZNF667-AS1, microRNA-1290 (miR-1290), and prune homolog 2 with BCH domain (PRUNE2) expression was determined with their relationship in cell biological processes analyzed also by means of gain- and loss-of-function assays. Xenograft mouse models were performed to re-produce the *in vitro* findings. We found a decline in ZNF667-AS1 expression in ESCC tissues and cell lines. ZNF667-AS1 overexpression indicated a favorable prognosis of ESCC sufferers. ZNF667-AS1 overexpression suppressed ESCC cell malignant potentials. ZNF667-AS1 reduced miR-1290 to result in upregulation of the miR-1290 target gene PRUNE2. The inhibiting property of ZNF667-AS1 on the malignant characteristics of ESCC cells was achieved by disrupting the miR-1290-mediated downregulation of PRUNE2. ZNF667-AS1 suppressed the tumorigenesis of ESCC *in vivo*. Collectively, our study demonstrates that ZNF667-AS1 can function as a tumor suppressor in ESCC by upregulating PRUNE2 and downregulating miR-1290.

Introduction

Esophageal squamous cell carcinomas (ESCC) is known as one of the deadliest human malignancies with the prominent features of late diagnosis, metastasis, treatment resistance, and commonly seen recurrence [1]. As a predominant type of esophageal cancer worldwide, ESCC accounts for more than 90% of all esophageal cancer cases in China [2]. Risk factors for ESCC include drinking, smoking, polycyclic aromatic hydrocarbons from various sources, high-temperature food, dietary factors, and poor oral health [3]. Accumulating evidence has unfolded aberrantly expressed long non-coding RNAs (lncRNAs) in the blood of cancer sufferers and exhibit significant potential as non-invasive tumor markers [4].

LncRNAs refer to a novel class of noncoding RNA longer than 200 nucleotides [5], and have been suggested to be of vital functionality in tumor development and progression [6,7]. For instance, knockdown of MALAT1 exerts inhibitory action in the progression of anaplastic thyroid carcinoma [8]. In particular, a decline of ZNF667-AS1 in detected in cervical cancer, and shows negative association with overall survival and tumor size [9]. In another example, downregulated ZNF667-AS1 causes an enhanced progression of laryngeal squamous cell carcinoma [10]. LncRNAs often act as competing endogenous RNA (ceRNA) to sponge microRNAs (miRs or miRNAs), thereby regulating the progression of cancers [11]. Exosome-mediated transfer of miR-1290 enhances malignant features of gastric cancer cells by targeting NKD1 [12]. A recent study has shown that ESCC sufferers with high serum miR-1290 levels present with a significantly worse survival [13], indicating that miR-1290 may be an appealing prognostic marker for ESCC. We also discovered the binding sites between miR-1290 and Prune homolog 2 (Drosophila) (PRUNE2) utilizing bioinformatics analysis. PRUNE2 is

Abbreviations: lncRNAs, long non-coding RNAs; PRUNE2, prune homolog 2 with BCH domain; ESCC, esophageal squamous cell carcinoma; miR-1290, microRNA-1290; ceRNA, competing endogenous RNA; RT-qPCR, Reverse transcription quantitative polymerase chain reaction; cDNA, complementary DNA; shRNA, short hairpin RNA; FISH, Fluorescent in situ hybridization.

* Corresponding authors.
E-mail addresses: yangdaokedr@163.com (D.-K. Yang), ldwang2007@126.com (L.-D. Wang).

https://doi.org/10.1016/j.tranon.2022.101371
Received 13 July 2021; Received in revised form 14 January 2022; Accepted 11 February 2022

known as a hypothetical paralog of PRUNE that is believed to suppress metastasis of tumor cells [14]. PRUNE2 exerts suppressive action in prostate cancer via its interaction with PCA3 [15]. Here, we hypothesized that ZNF667-AS1 may be involved in the ESCC progression through its possible interplay with miR-1290-mediated PRUNE2.

Materials and methods

Ethics statement

All participants supplied written informed consent prior to inclusion. The study protocol was ratified by the Ethic Committee of The First Affiliated Hospital of Zhengzhou University and was compliant with the *Declaration of Helsinki*. The animal experiments were implemented in the light of the recommendations in the Guide for the Care and Use of Laboratory Animals of the National Institutes of Health. The animal experiment protocols were ratified by the Institutional Animal Care and Use Committee of The First Affiliated Hospital of Zhengzhou University.

Sample collection and cell lines

From January 2015 to December 2017, 70 ESCC specimens were obtained from the patients with ESCC (41 males and 29 females; aged 45.60 ± 9.28 years) who were hospitalized and received treatment at the department of General Surgery of The First Affiliated Hospital of Zhengzhou University. All subjects had not received any treatment prior to surgery. All surgical specimens were gained from the non-necrotic and bleeding area from the center of the ESCC-affected tissue and the distal esophageal normal mucosa, and immediately stored in a −80 °C refrigerator. Human ESCC cell lines Eca109 (CL0092, Fenghui Biotech Co., Ltd., Human, China), TE-1 (CL0314, Fenghui), EC-1 (24,951, American Type Culture Collection [ATCC], Manassas, VA, USA) and Siha (HTB-35, ATCC) and the normal esophageal epithelial cell line HET-1A (CRL-2692, Fenghui) were included in this study.

Bioinformatics analysis

Two gene expression datasets (GSE45670 and GSE45168) and two miRNA expression datasets (GSE55856 and GSE43732) gained from Gene Expression Omnibus (GEO) database were utilized for differential analysis (Supplementary Table 1). The R package 'affy' was utilized for standardized pretreatment of microarray expression data [16], and 'limma' was used to collect differentially expressed genes/miRNAs, with $|\log2FC| > 2.0$, adj.*p*.Val < 0.05 as the screening criteria [17]. A heat map of differentially expressed genes/miRNAs was plotted. Based on the differential analysis of GSE45670 dataset, we focused on the differential expression of ZNF667-AS1 in ESCC, and further analyzed its potential role in ESCC. The LncATLAS database provided a large set of subcellular localization data pertaining to lncRNAs [18], and was applied for searching the subcellular localization of differentially expressed lncRNAs. The RNA22 tool was used for identifying miRNA binding sites and their corresponding heterogeneous complexes [19]. miRNAs that ZNF667-AS1 might bind to were thus predicted by means of the RNA22 tool. Jvenn was employed to compare the predicted miRNAs with the differentially expressed miRNAs from miRNA expression datasets, in order to identify differentially expressed miRNAs that might be bound by ZNF667-AS1. Target genes possibly bound by differentially expressed miRNAs were predicted using RNA22, DIANA, mirDIP, TargetScan, miRWalk and miRDB databases. TargetScan database was used to predict the binding site between miRNAs and the predicted target genes.

RNA extraction and mRNA reverse transcription

Total RNA was extracted from human esophageal squamous cells, esophageal carcinoma tissues and normal mucosa of distal esophagus using TRIzol reagent. All cells were lysed with 1 mL Trizol lysis buffer (Invitrogen Inc., Carlsbad, CA, USA) and collected in eppendorf (EP) tubes. A small portion of tissues were collected and lysed with 1 mL TRIzol lysis buffer and later with an electric tissue grinder (TIANGEN Biotechnology Co., Ltd, Beijing, China). Cells and tissues after lysis were treated with 200 μL chloroform for 15 s and centrifuged at 12,000 × g and 4 °C for 20 min. Then, the upper aqueous phase was transferred into another EP tube, followed by treatment utilizing 500 μL isopropanol and centrifugation at 12,000 × g and 4 °C for 20 min to remove the supernatant. The white precipitate on the bottom was washed with 1 mL 75% ethanol, centrifuged at 12,000 × g and 4 °C for 15 min and air-dried until it became completely transparent. Subsequently, RNA was dissolved in 20 - 50 μL RNase-free water, followed by concentration measurement by means of NANO DROP 2000 spectrophotometer (Thermo, Scientific, Rockford, IL, USA). ReverTra Ace® qPCR RT Master Mix with gDNA Remover (TOYOBO, Tokyo, Japan) kit was used for reverse transcription of RNA into complementary DNA (cDNA). For miRNA detection, PolyA Tailing Reverse Transcription Kit (B532451, Sangon Biotech Co., Ltd., Shanghai, China) was utilized for reverse transcription, with PolyA-containing cDNA obtained. The reverse transcription system was 20 μL with 500 ng RNA.

Reverse transcription quantitative polymerase chain reaction (RT-qPCR)

The primers of ZNF667-AS1, miR-1290 and PRUNE2 were synthesized by Sangon (Shanghai, China) (Supplementary Table 2). The synthesized cDNA was used as a template for RT-qPCR. The fluorescent quantitation PCR was performed using a 2 × RealStar Green Mixture (GenStar, San Diego, CA, USA) on a Bio-Rad CFX96 Touch™ fluorescent quantitative PCR system. Glyceraldehyde-3-phosphate dehydrogenase (GAPDH) was used as the internal reference for quantifying ZNF667-AS1 and PRUNE2, whereas U6 for miR-1290. The relative mRNA expression of the target gene was calculated by $2^{-\Delta\Delta Ct}$ method.

Cell treatment

Siha and Eca109 cells were manipulated with the plasmids of overexpression (oe)-ZNF667-AS1, short hairpin RNA (sh)-ZNF667-AS1, oe-PRUNE2 and sh-PRUNE2 as well as miR-1290 mimic and miR-1290 inhibitor alone or in combination. The above plasmids, mimic, and inhibitor were purchased from Sino-American Biotechnology Co., Ltd. (Beijing, China). The cells were plated into a six-well plate at 24 h before transfection, and the plasmids, mimic, and inhibitor were transiently transfected into ESCC cells utilizing Lipofectamine 2000 transfection reagent (Invitrogen) upon 80% confluency for 6 h. After another 48 h of culturing, the cells were chose for subsequent experiments.

Colony forming assay

Siha and Eca109 cells were submitted to 0.25% trypsin detachment to prepare a single cell suspension for cell counting with the cell density adjusted (1×10^6 cells/L). Based on the experimental requirements, cells was plated in a dish containing 10 mL medium preheated at 37 °C at a density of 50, 100, and 200 cells/dish, respectively. Next, the cells were evenly distributed and cultured at 37 °C with 5% CO_2 for 2 - 3 weeks. Termination of the culture was implemented when the cell colony was visible. Thereafter, the cells were fixed with 5 mL 4% paraformaldehyde for 15 min, and stained by GIMSA dye liquor (Invitrogen) for 10 - 30 min. The cell colony number was observed by microscopic examination. The rate of colony formation = the colony number / the plated cell number.

Flow cytometry

Cells were plated into 6-well plates (2×10^5 cells/well). After 72 h of transfection, the cells were trypsinized and centrifuged at 800 × g with the supernatant discarded. In the light of the Annexin V-FITC Apoptosis

Detection Kit (BD Biosciences, Franklin Lakes, NJ), the cells were resuspended in 500 mL buffer solution and incubated with 5 μL FITC and 5 μL PI for 15 min. Assessment of cell apoptosis was implemented by a BD FACSCalibur flow cytometer.

Western blot analysis

Total protein was extracted with the concentration determined by bicinchoninic acid method (Pierce Biotechnology Inc, Rockford, IL). After separation utilizing electrophoresis, the protein was transferred onto a polyvinylidene fluoride membrane which was blocked with 5% skim milk for 1 h. Incubation of membrane was implemented with primary antibodies against PRUNE2 (PA5–100,310, 1:1000, Invitrogen), N-cadherin (ab76011, 1:1000, Abcam Inc., Cambridge, UK), E-cadherin (ab231303, 1:1000, Abcam), Bcl-2 (ab182858, 1:1000, Abcam), Bax (ab32503, 1:1000, Abcam), caspase-3 (ab184787, 1:1000, Abcam), and cleaved caspase-3 (ab32042, 1:1000, Abcam) as well as secondary antibody horseradish peroxidase (HPR)-conjugated immunoglobulin G (IgG). The immunocomplexes on the membrane were visualized utilizing ECL reagent and analyzed by the Bio-Rad ChemiDoc™ imaging system. With GAPDH as an internal control, the protein imprinted image was analyzed using ImageJ2x software.

Fluorescent in situ hybridization (FISH)

Information about the subcellular localization of ZNF667-AS1 was gained with the help of a bioinformatics tool (http://lncatlas.crg.eu/). The subcellular localization of ZNF667-AS1 in Eca109 and Siha cells was verified by FISH performed using the Ribo™ lncRNA FISH Probe Mix (Red) (Guangzhou RiboBio Co., Ltd., Guangdong, China), with circular RNA TMEM87A and U2 snDNA as controls [20]. Five different visual fields were randomly selected for observation and photographing under a fluorescence microscope (Olympus Corporation, Tokyo, Japan)

RNA pull-down assay

Eca109 and Siha cells were transfected with Bio-miR-NC and Bio-miR-1290. The cells were then harvested and lysed with RIP lysis buffer (Millipore, Billerica, MA, USA). miRNAs were screened by adsorption of magnetic beads coated with streptavidin, and the enrichment of ZNF667-AS1 was detected by RT-qPCR.

Luciferase assay

The predicted binding site and mutant (MUT) fragments of ZNF667-AS1 and miR-1290 were inserted into luciferase reporter vectors as reporter plasmids ZNF667-AS1-wild type (WT) and ZNF667-AS1-MUT. Negative control (NC) and miR-1290 mimic were co-transfected with ZNF667-AS1 luciferase reporter plasmids into 293T cells (Oulu Biotecnology, Co., Ltd, Shanghai, China.) to detect whether ZNF667-AS1 could bind to miR-1290. A luciferase detection kit (K801–200, BioVision, Milpitas, CA) and Dual Luciferase Reporter Gene Assay System (Promega Corporation, Madison, WI) were used to detect luciferase reporter genes. Additionally, the predicted binding site and MUT fragments of PRUNE2 and miR-1290 were inserted into luciferase reporter vectors as reporter plasmids PRUNE2-WT and PRUNE2-MUT. NC and miR-1290 mimic were co-transfected with PRUNE2 luciferase reporter plasmids to determine whether PRUNE2 could bind to miR-1290. The specific methods and steps were the same as above.

Transwell assay

Siha and Eca109 cell invasion was assessed with the help of a 8-μm Transwell chamber (Corning Glass Works, Corning, N.Y., USA) with matrigel (Sigma-Aldrich) [21]. Counting of stained cells was implemented under an inverted microscope with five randomly selected visual fields.

Scratch test

Siha and Eca109 cells following different treatment were plated in 6-well plates (5×10^5 cells/well). Upon adherence, scratches were created using a 2-mm cell scraper from the middle of each well and then 24 h of culturing was carried out. The images were taken at 0 h and 24 h after scratch test, and the Image ProPlus software 6.0 was used to calculate the scratch healing rate.

Xenograft tumor in nude mice

GFPSpark® lentiviruses (Sino-American Biotechnology Co. Ltd., Beijing, China) embedded plasmids were transduced into Siha cells for 48 h according to multiplicity of infection (MOI) = 40, 80, or 100. Then, the stable cell lines were selected for induction of xenograft tumor in nude mice. Siha cell suspension (1×10^6 cells/μL) was made utilizing Serum-free RPMI 1640 medium (Gibco). Twenty six-week-old specific pathogen-free (SPF) male nude mice (weighing 18 - 22 g; Shanghai SLAC Laboratory Animal Co., Ltd., Shanghai, China) were randomly divided into two groups (10 mice in each group). The tumorigenic experiment lasted for 4 weeks. After anesthesia with ether, the nude mice were disinfected. Thereafter, stably transfected ESCC cells (transfected with oe-NC and oe-ZNF667-AS1) were inoculated subcutaneously into the back of the right hind leg at a concentration of 1×10^6 (200 μL). The mice were fed under the same environment. After the tumor formed, the measurement of length and width of the tumor was implemented every two days, followed by calculation of tumor volume and weighing.

Immunohistochemistry

Clinical tissue specimens were embedded in paraffin, dewaxed with xylene, hydrated with alcohol gradient, and washed with tap water for 2 min. Then endogenous peroxidase was blocked by 3% methanol-H_2O_2 for 20 min. Antigen retrieval was implemented in a water bath. After that, the sections were blocked with normal goat serum (Shanghai Haoran Biological Technology Co., Ltd, Shanghai, China) and incubated with primary antibodies against PRUNE2 (PA5–56,632, 1:200, Invitrogen), E-cadherin (ab231303, 1:200, Abcam), and N-cadherin (ab76011, 1: 300, Abcam) overnight at 4 °C. The next day, the sections were re-probed with secondary antibody of goat anti-rabbit IgG (ab6785, 1: 1000, Abcam) at 37 °C for 20 min, followed by treatment with HPR-labeled streptavidin protein working solution (0343–10,000 U, Imunbio Technology Co., Ltd, Beijing, China) at 37 °C for 20 min. Thereafter, the sections were photographed under a microscope in five randomly selected high-power fields.

Statistical analysis

All data were analyzed by means of SPSS 21.0 software (IBM Corp, Armonk, NY, USA). Measurement data are presented with mean ± standard deviation. If the data conformed to normal distribution and homogeneous variance, paired *t*-test was used to compare the data between two groups with paired design and unpaired *t*-test was applied under unpaired design. Comparison of data between multiple groups was performed using one-way analysis of variance (ANOVA) with Tukey's post hoc test. The data among multiple groups at different time points were analyzed by Bonferroni-corrected repeated measures ANOVA. A p less than 0.05 was concluded as statistically significant.

Results

ZNF667-AS1 expresses at a low level in ESCC

Supplementary Figure 1 presents a heat map of the first 30

differentially expressed lncRNAs following analysis of the ESCC-related GSE45670 dataset. A box plot showed decreased ZNF667-AS1 expression in ESCC samples (n= 25) compared with control samples (n= 10) (Fig. 1A). Meanwhile, downregulated ZNF667-AS1 expression was also seen in ESCC tissues and four ESCC cell lines Eca109, TE-1, EC-1 and Siha (Fig. 1B, C). The Siha cell line showed the lowest ZNF667-AS1 expression than the other three ESCC cell lines (Fig. 1C). Therefore, the Siha and Eca109 cell lines, which showed relatively low ZNF667-AS1 expression, were chose for the subsequent experiments.

The subcellular localization of ZNF667-AS1 was identified to be expressed in the cytoplasm using the LncATLAS database (Fig. 1D). A recent study has reported that circular RNA TMEM87A is localized in the cytoplasm of human gastric cancer cells BGC823 and MKN45 [22]. U2 snDNA has been shown to be localized in the nucleus [23]. On the basis of previous reports, we used circular RNA TMEM87A and U2 snDNA as controls. In Siha and Eca109 cells, circular RNA TMEM87A was found to be localized in the cytoplasm, while U2 snDNA in the nucleus. ZNF667-AS1 in this study also demonstrated a cytoplasmic distribution (Supplementary Figure 2). Thereafter, 70 ESCC sufferers were divided into two groups based on the median ZNF667-AS1 expression: high expression group (ZNF667-AS1 expression > median, 35) and low expression group (ZNF667-AS1 expression < median, 35) (Fig. 1E). Kaplan-Meier analysis depicted that the survival rate of patients with poor expression of ZNF667-AS1 was lower than those with high expression of ZNF667-AS1 (log rank = 7.80, p= 0.015) (Fig. 1F), implying a negative association between ZNF667-AS1 and the prognosis of ESCC patients.

ZNF667-AS1 inhibits ESCC cell malignant potentials in vitro

Siha and Eca109 cells were manipulated with oe-ZNF667-AS1 and sh-ZNF667-AS1, with the transfection efficiency confirmed by RT-qPCR (Fig. 2A). As shown in Fig. 2B, C, transfection of oe-ZNF667-AS1 plasmid reduced the number of cell clones and enhanced cell apoptosis. However, transfection with sh-ZNF667-AS1 plasmid led to opposite results. Besides, overexpression of ZNF667-AS1 increased the ratio of cleaved caspase-3/caspase 3 while silencing of ZNF667-AS1 decreased the ratio of cleaved caspase3/caspase 3 (Fig. 2D, Supplementary Figure 3A). Moreover, transfection with oe-ZNF667-AS1 limited the migrative and invasive properties of Siha and Eca109 cells but transfection with sh-ZNF667-AS1 induced contrary results (Fig. 2E, F, Supplementary Fig. 3B, C).

ZNF667-AS1 competitively binds to miR-1290 and reduces its expression in ESCC cells

We then further depicted the mechanisms of ZNF667-AS1 involvement in ESCC. Through RNA22 database, 651 miRNAs that may bind by ZNF667-AS1 were found. Additionally, 12 and 6 differentially expressed miRNAs were identified from datasets GSE55856 and GSE43732, respectively. Based on the comparison of the results of target miRNAs of ZNF667-AS1 with the differentially expressed miRNAs using a Venn diagram, an overlapping miRNA hsa-miR-1290 (Fig. 3A) was identified. A box plot of the expression data of miR-1290 exhibited higher expression of miR-1290 in ESCC samples (Fig. 3B). Meanwhile, elevation of miR-1290 expression was also seen in ESCC tissues and four ESCC cell lines Eca109, TE-1, EC-1 and Siha (Fig. 3C, D), which was opposite to the expression of ZNF667-AS1. Therefore, it could be speculated that

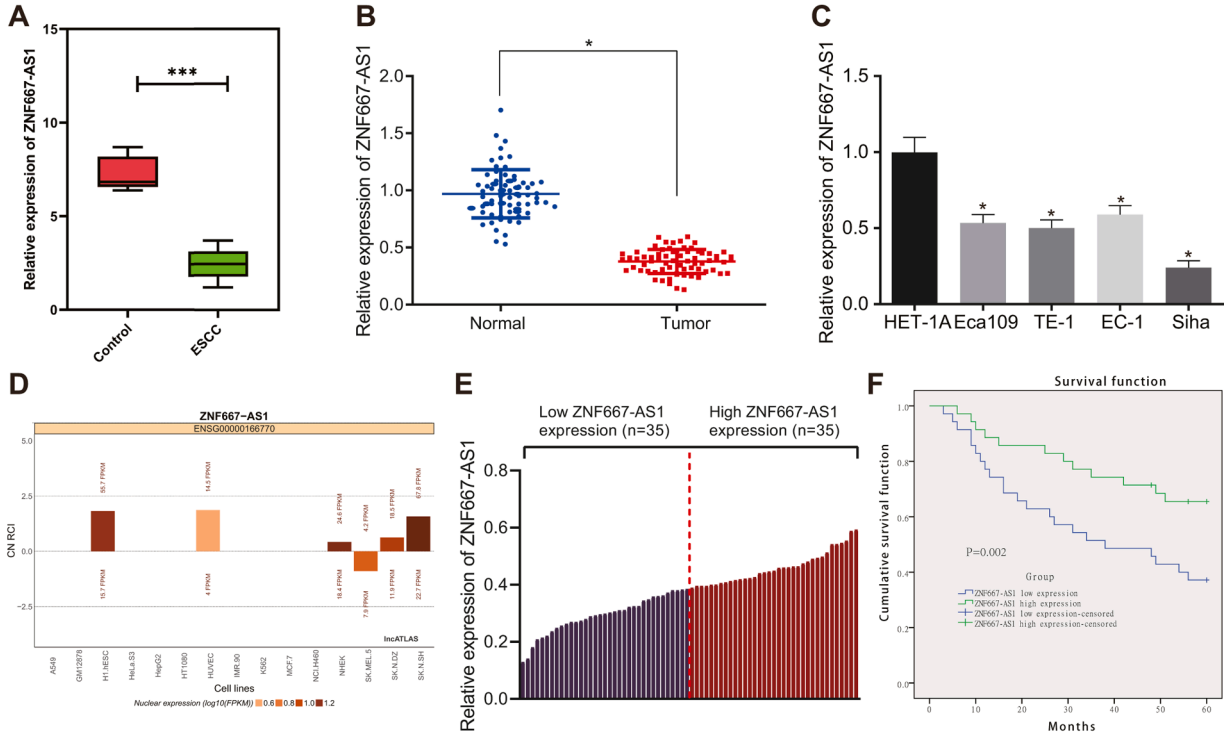

Fig. 1. ZNF667-AS1 expresses poorly in ESCC. A, A box plot of ZNF667-AS1 expression in control samples (n = 10) and ESCC samples (n = 25) in the GSE45670 dataset. B, ZNF667-AS1 expression in ESCC and adjacent normal tissues (n = 70) as determined by RT-qPCR. * p < 0.05, compared with adjacent normal tissues. C, The expression of ZNF667-AS1 in human normal esophageal epithelial cell line HET-1A, and ESCC cell lines Eca109, TE-1, EC-1 and Siha determined by RT-qPCR. * p < 0.05, compared with HET-1A cell line. D, Subcellular localization of ZNF667-AS1 predicted by the LncATLAS database. E, Division of ESCC patients into high expression group (ZNF667-AS1 expression > median, 35) and low expression group (ZNF667-AS1 expression < median, 35) according to the median value of ZNF667-AS1 expression: (n= 70). F, Kaplan-Meier survival analysis (log-rank test) based on ZNF667-AS1 expression (n= 70). Statistical data are measurement data, and summarized as mean ± standard deviation. Comparison of data between two groups was conducted by paired t-test and that between multiple groups using one-way ANOVA with Tukey's post hoc test. Cell experiment was repeated three times independently.

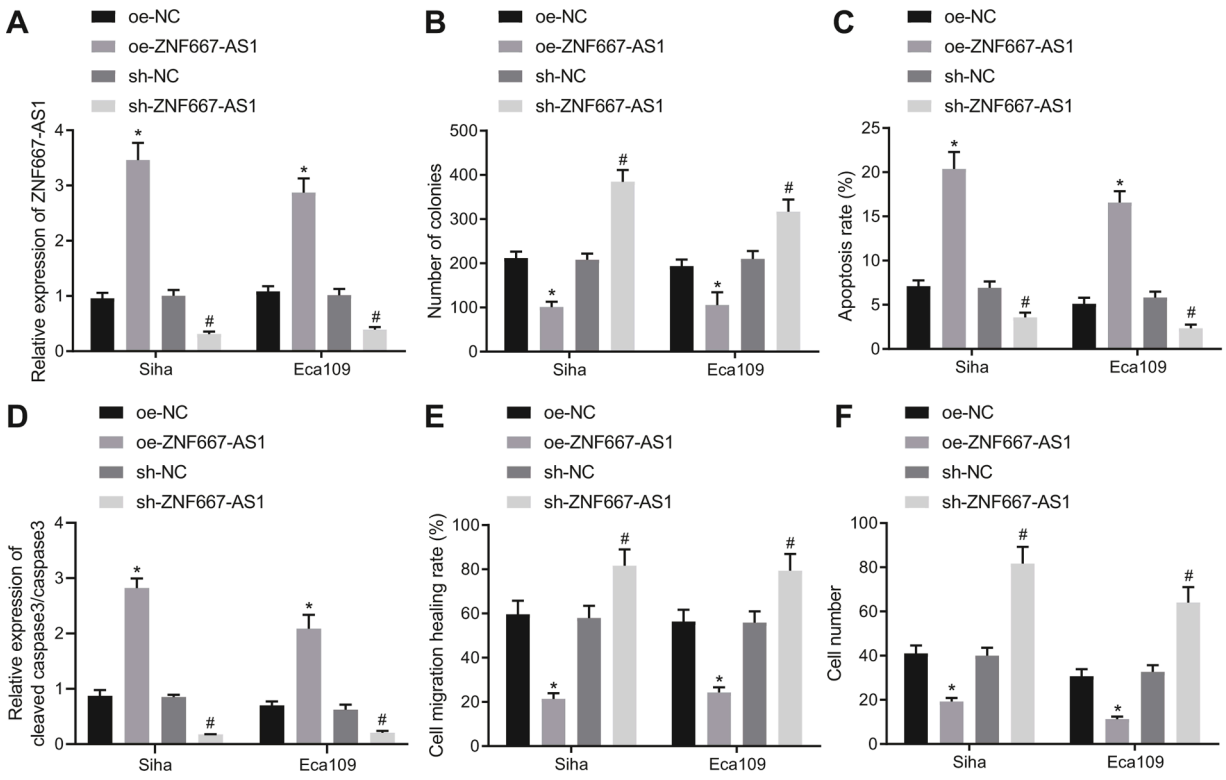

Fig. 2. ZNF667-AS1 impairs the proliferation, migration, and invasion and enhances apoptosis in Siha and Eca109 cells *in vitro*. Siha and Eca109 cells were treated with the plasmids of oe-ZNF667-AS1 and sh-ZNF667-AS1. A, ZNF667-AS1 expression in Siha and Eca109 cells determined by RT-qPCR. B, Clonogenic potential of Siha and Eca109 cells assessed by colony forming assay. C, Apoptosis of Siha and Eca109 cells measured by flow cytometry. D, Western blot analysis of caspase-3 and cleaved caspase-3 proteins in Siha and Eca109 cells. E, Migration ability of Siha and Eca109 cells assessed by scratch test. F, Invasion ability of Siha and Eca109 cells measured by Transwell assay. *, $p < 0.05$ *vs.* the transfection of oe-NC plasmid; #, $p < 0.05$ *vs.* the transfection of sh-NC plasmid. Measurement data are summarized as mean ± standard deviation. Comparison of data between two groups was conducted by unpaired *t*-test. Cell experiment was repeated three times independently.

ZNF667-AS1 might sponge miR-1290 in ESCC.

Specific binding sites of ZNF667-AS1 and miR-1290 were predicted using RNA22 (Fig. 3E), which was verified by luciferase assay that miR-1290 mimic reduced the luciferase activity of ZNF667-AS1-WT ($p < 0.05$) without altering that of ZNF667-AS1-MUT ($p > 0.05$) (Fig. 3F). Besides, the enrichment of ZNF667-AS1 was increased in the presence of Bio-miR-1290 (Fig. 3G). Furthermore, functional assays demonstrated that overexpression of ZNF667-AS1 inhibited Siha and Eca109 cell migration and invasion, which was reversed by further elevation of miR-1290 (Fig. 3H, I).

ZNF667-AS1 upregulates the expression of PRUNE2 by sponging miR-1290

Searching from RNA22, DIANA, mirDIP, TargetScan, MicroWalk and MicroDB databases identified 10,075, 1367, 344, 4599, 1687, and 377 target genes of miR-1290, respectively. Following Venn diagram of these genes, 9 genes (ARID4B, ACSL4, PRUNE2, CBFA2T3, UNC79, HIGD2A, BPTF, ERBB4, and SH2D1A) were found at the intersection (Fig. 4A), suggesting that these specific genes were highly likely to be regulated by miR-1290. Additionally, 732 and 642 differentially expressed genes were identified from the GSE45670 and GSE45168 datasets, respectively. Comparison of these differentially expressed genes with the predicted target genes showed one common gene, PRUNE2 (Fig. 4B). PRUNE2 expression data were then extracted from the GSE45670 dataset and a box plot was drawn where the expression of PRUNE2 was lower in ESCC samples than that in control samples (Fig. 4C). Next, RT-qPCR data was confirmatory, showing a reduction in PRUNE2 in ESCC tissues (Fig. 4D) and cell lines Eca109, TE-1, EC-1 and Siha (Fig. 4E). Based on these results, it was speculated that PRUNE2 was a target gene of miR-1290 in ESCC.

To confirm this speculation, TargetScan was used for bioinformatics prediction of the binding site between PRUNE2 and miR-1290 (Fig. 4F), which was also validated by luciferase assay that miR-1290 mimic caused a reduction in the luciferase activity of PRUNE2-WT while led to no alteration in PRUNE2-MUT (Fig. 4G). In addition, an elevation in PRUNE2 and ZNF667-AS1 expression yet a decline in that of miR-1290 were seen following oe-ZNF667-AS1. However, opposite results were noted in the presence of miR-1290 mimic. The expression of PRUNE2 and ZNF667-AS1 was higher in cells treated with oe-ZNF667-AS1 + miR-1290 mimic than that in cells treated with miR-1290 mimic alone, but lower than that in those with single oe-ZNF667-AS1 plasmid. Moreover, the expression of miR-1290 was elevated in the presence of oe-ZNF667-AS1 + miR-1290 mimic *versus* oe-ZNF667-AS1 alone while it was reduced as compared to miR-1290 mimic alone (Fig. 4H, I). Meanwhile, the expression of ZNF667-AS1 and PRUNE2 was decreased while that of miR-1290 was enhanced in response to sh-ZNF667-AS1; opposite results were found following transfection with miR-1290 inhibitor (Fig. 4J, K).

ZNF667-AS1 represses the malignant phenotypes of ESCC cells by binding to miR-1290 and elevating PRUNE2

Next, we sought to elucidate the effect of PRUNE2 on ESCC. Siha cells were manipulated with sh-ZNF667-AS1 and oe-ZNF667-AS1. RT-qPCR and Western blot analysis conformed their transfection efficiency, as evidenced by decreased PRUNE2 expression in Siha cells transfected with sh-ZNF667-AS1–1, sh-ZNF667-AS1–2 or sh-ZNF667-AS1–3 yet increased PRUNE2 expression upon transfection with oe-ZNF667-AS1. sh-ZNF667-AS1–1 showed the superior efficiency and was thus chosen

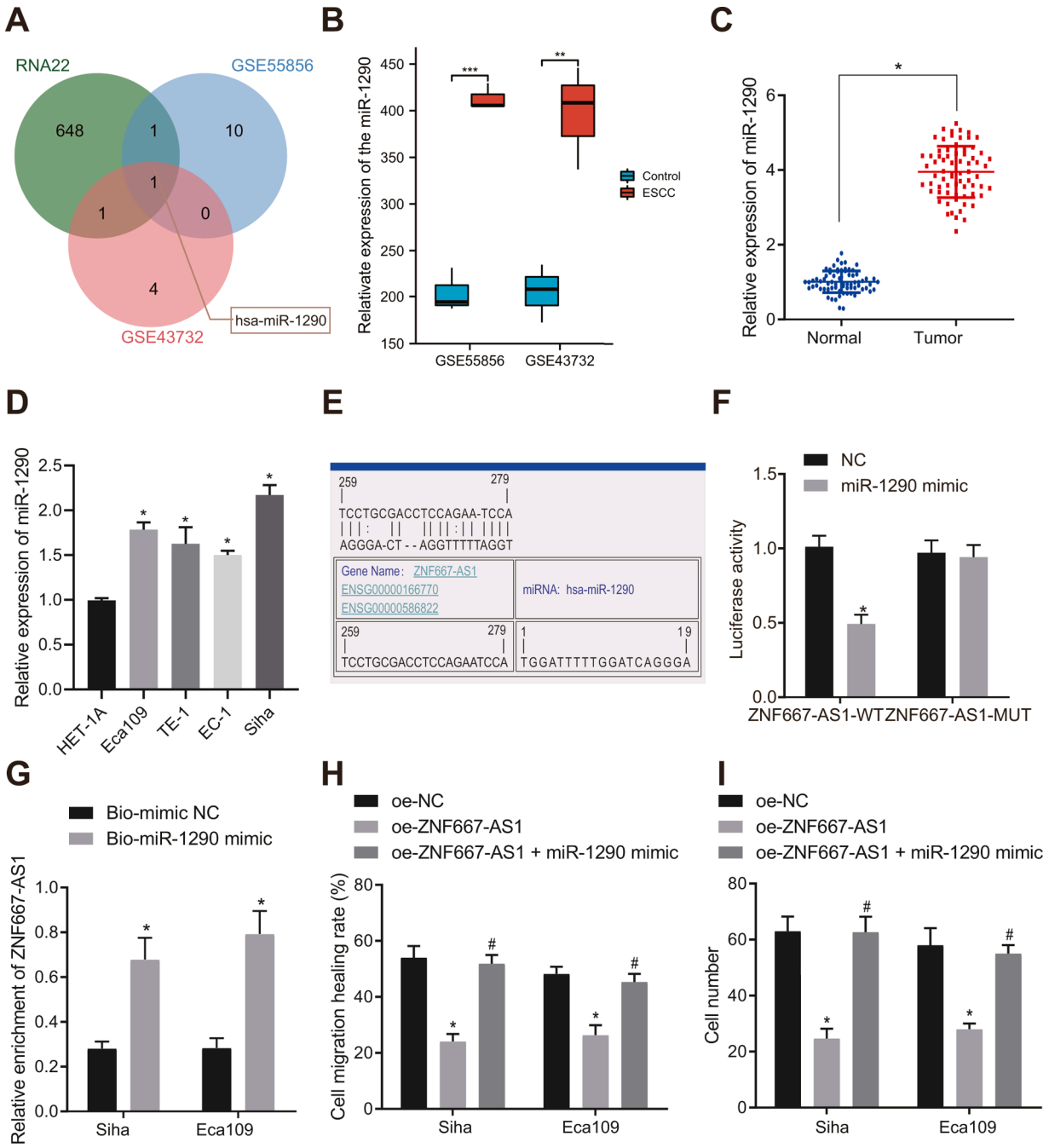

Fig. 3. ZNF667-AS1 binds to miR-1290 and downregulates its expression in ESCC cells, thus repressing the malignant characteristics of ESCC cells. A, Venn diagram of target miRNAs of ZNF667-AS1 predicted by RNA22 and differentially expressed miRNAs from miRNA expression datasets GSE55856 and GSE43732. B, A box plot of miR-1290 expression in control samples and ESCC samples in the ESCC-related GSE55856 ($n = 108$ for control samples and $n = 108$ for ESCC samples) and GSE43732 ($n = 119$ for control samples and $n = 119$ for ESCC samples) datasets. C, The expression of miR-1290 in ESCC tissues and adjacent normal tissues ($n= 70$) determined by RT-qPCR. *, $p < 0.05$ *vs.* the adjacent normal tissues. D, The expression of miR-1290 in human normal esophageal epithelial cell line HET-1A, and ESCC cell lines Eca109, TE-1, EC-1 and Siha determined by RT-qPCR. * $p < 0.05$, compared with HET-1A cell line. E, Binding sites between ZNF667-AS1 and miR-1290 predicted by RNA22. F, Binding of ZNF667-AS1 to miR-1290 in 293T cells confirmed by dual-luciferase report assay. * $p < 0.05$, compared with NC-transfected 293T cells. G, RNA pull-down assay analysis of the presence of ZNF667-AS1 and miR-1290 in the same complex in Siha and Eca109 cells transfected with Bio-miR-NC or Bio-miR-1290. Siha and Eca109 cells were treated with the plasmid of oe-ZNF667-AS1 and miR-1290 mimic. H. The migration of Siha and Eca109 cells assessed by scratch test. I, Invasion ability of Siha and Eca109 cells measured by Transwell assay. *, $p < 0.05$ *vs.* cells transfected with oe-NC plasmid; #, $p < 0.05$ *vs.* cells transfected with oe-ZNF667-AS1. Statistical data are measurement data, and summarized as mean ± standard deviation. Comparison of data between two groups was conducted using unpaired *t*-test and that between multiple groups using one-way ANOVA with Tukey's post hoc test. Cell experiment was repeated three times independently.

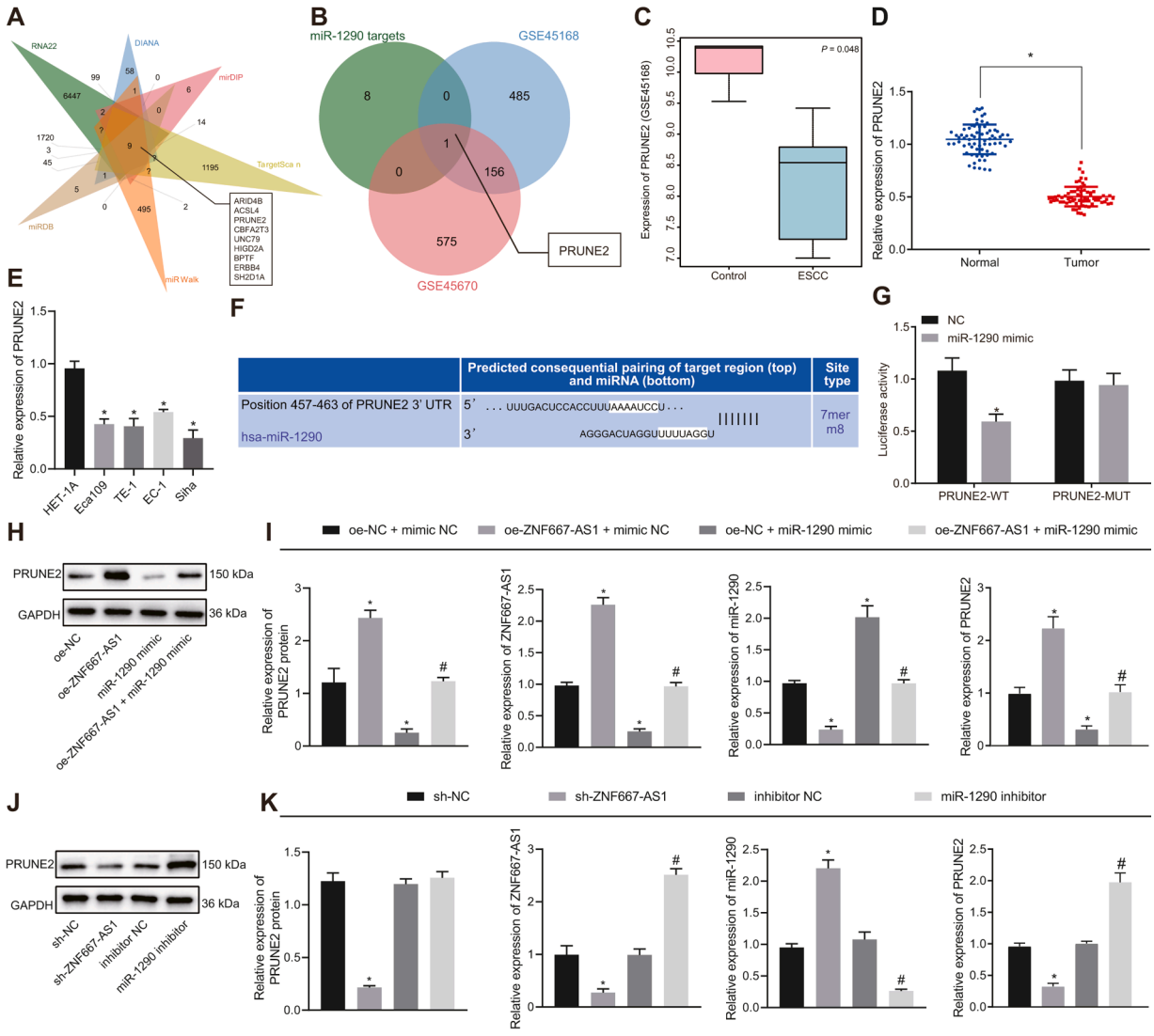

Fig. 4. ZNF667-AS1 upregulates the expression of PRUNE2 by sponging miR-1290. A, Venn diagram of the target genes of miR-1290 predicted using RNA22, DIANA, mirDIP, TargetScan, MicroWalk and MicroDB databases. B, Venn diagram of the 9 overlapping target genes of miR-1290 and differentially expressed genes obtained from GSE45670 and GSE45168 datasets. C, A box plot of PRUNE2 expression in control samples (n= 4) and ESCC samples (n= 4) in the ESCC-related GSE45670 dataset. D, RT-qPCR analysis of the expression of PRUNE2 in ESCC tissues and adjacent normal tissues (n= 70). * $p < 0.05$ *vs.* adjacent normal tissues. E, The expression of PRUNE2 in human normal esophageal epithelial cell line HET-1A, and ESCC cell lines Eca109, TE-1, EC-1 and Siha determined by RT-qPCR. * $p < 0.05$, compared with HET-1A cell line. F, Putative miR-1290 binding sites in the 3′UTR of PRUNE2 mRNA predicted by RNA22. G, Binding of miR-1290 to PRUNE2 in 293T cells confirmed by dual-luciferase report assay. * $p < 0.05$, compared with NC-transfected 293T cells. H, Western blot analysis of PRUNE2 protein in Siha and Eca109 cells transfected with plasmids of oe-ZNF667-AS1, miR-1290 mimic or both. I, RT-qPCR detection of the expression of ZNF667-AS1, PRUNE2 and miR-1290 in Siha and Eca109 cells transfected with plasmids of oe-ZNF667-AS1, miR-1290 mimic or both. J, Western blot analysis of PRUNE2 protein in Siha and Eca109 cells transfected with plasmids of sh-ZNF667-AS1 or miR-1290 inhibitor. K, RT-qPCR detection of the expression of ZNF667-AS1, PRUNE2 and miR-1290 in Siha and Eca109 cells transfected with plasmids of sh-ZNF667-AS1 or miR-1290 inhibitor. * $p < 0.05$ *vs.* the transfection of oe-NC + mimic NC or sh-NC plasmids. # $p < 0.05$ *vs.* the transfection of oe-ZNF667-AS1 + mimic NC or inhibitor NC plasmids. Statistical data are measurement data, and summarized as mean ± standard deviation. Comparison of data between two groups was conducted using unpaired *t*-test and that between multiple groups using one-way ANOVA with Tukey's post hoc test. Cell experiment was repeated three times independently.

for the follow-up experiments (Supplementary Figure 4A, B). Then, we found that the Siha and Eca109 cell migration and invasion were augmented upon sh-PRUNE2 transfection, the effect of which was reversed by oe-PRUNE2 (Supplementary Figure 4C, D). In addition, in the presence of oe-ZNF667-AS1 or miR-1290 inhibitor, the migration and invasion were decreased in Siha and Eca109 cells, which were abrogated by treatment with oe-ZNF667-AS1 + sh-PRUNE2 or miR-1290 inhibitor + sh-PRUNE2 (Fig. 5A, B, Supplementary Figure 5A, B).

ZNF667-AS1 limits the tumorigenesis of ESCC in vivo

Finally, a xenograft model of ESCC was constructed. The volume of tumor grown as xenografts was measured every week. After four weeks, the tumor was removed and weighed after which the tumor volume was calculated. The results showed that tumorigenesis of ESCC was inhibited as evidenced by the reduced tumor weight and volume in mice bearing cells expressing oe-ZNF667-AS1 (Fig. 6A–C). Additionally, mice bearing cells expressing oe-ZNF667-AS1 had elevated PRUNE2 and E-cadherin along with decreased N-cadherin in the tumor tissues (Fig. 6D–F), which showed inhibited migration ability of tumor cells and deterioration of tumors. Furthermore, the expression of Ki-67 was diminished in the tumor tissues of mice treated with oe-ZNF667-AS1 (Fig. 6G), indicating that ZNF667-AS1 overexpression inhibited the proliferation of tumor cells. In the meantime, reductions in the expression of N-cadherin, Bcl-2

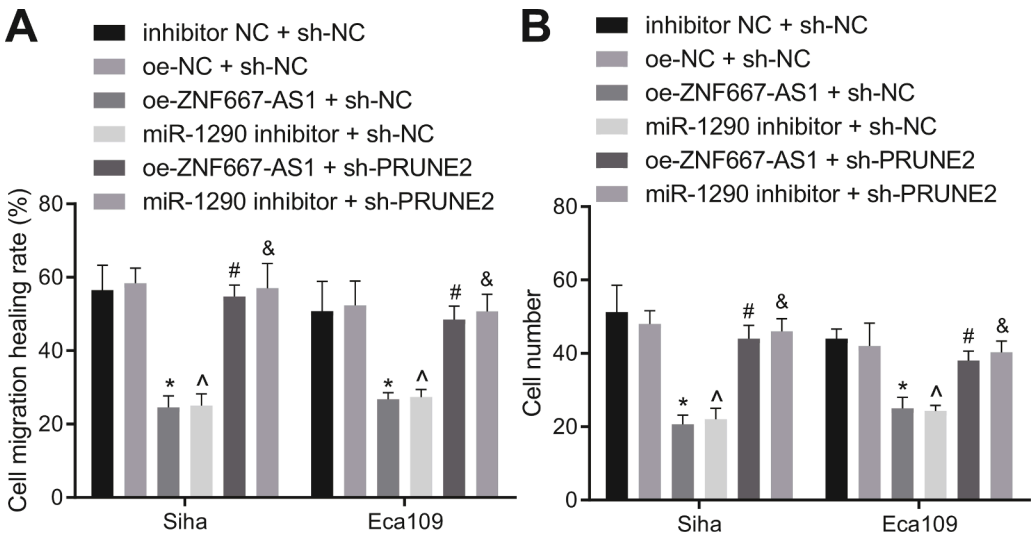

Fig. 5. ZNF667-AS1 impairs the malignant phenotypes of ESCC cells through PRUNE2 upregulation and miR-1290 reduction. Siha and Eca109 cells transfected with plasmids of oe-ZNF667-AS1, miR-1290 inhibitor, oe-PRUNE2, and sh-PRUNE2 alone or in combination. A, The migration ability of Siha and Eca109 cells measured by scratch test. B, The invasion ability of Siha and Eca109 cells measured by Transwell assay. * $p < 0.05$, *vs.* Siha and Eca109 cells transfected with oe-NC + sh-NC; ^ $p < 0.05$, *vs.* Siha and Eca109 cells transfected with inhibitor NC + sh-NC; # $p < 0.05$, *vs.* Siha and Eca109 cells transfected with oe-ZNF667-AS1 + sh-NC. & $p < 0.05$, *vs.* Siha and Eca109 cells transfected with miR-1290 inhibitor + sh-NC. Statistical data are measurement data and summarized as mean ± standard deviation. Comparison of data between multiple groups was conducted using one-way ANOVA with Tukey's post hoc test. Cell experiment was repeated three times independently.

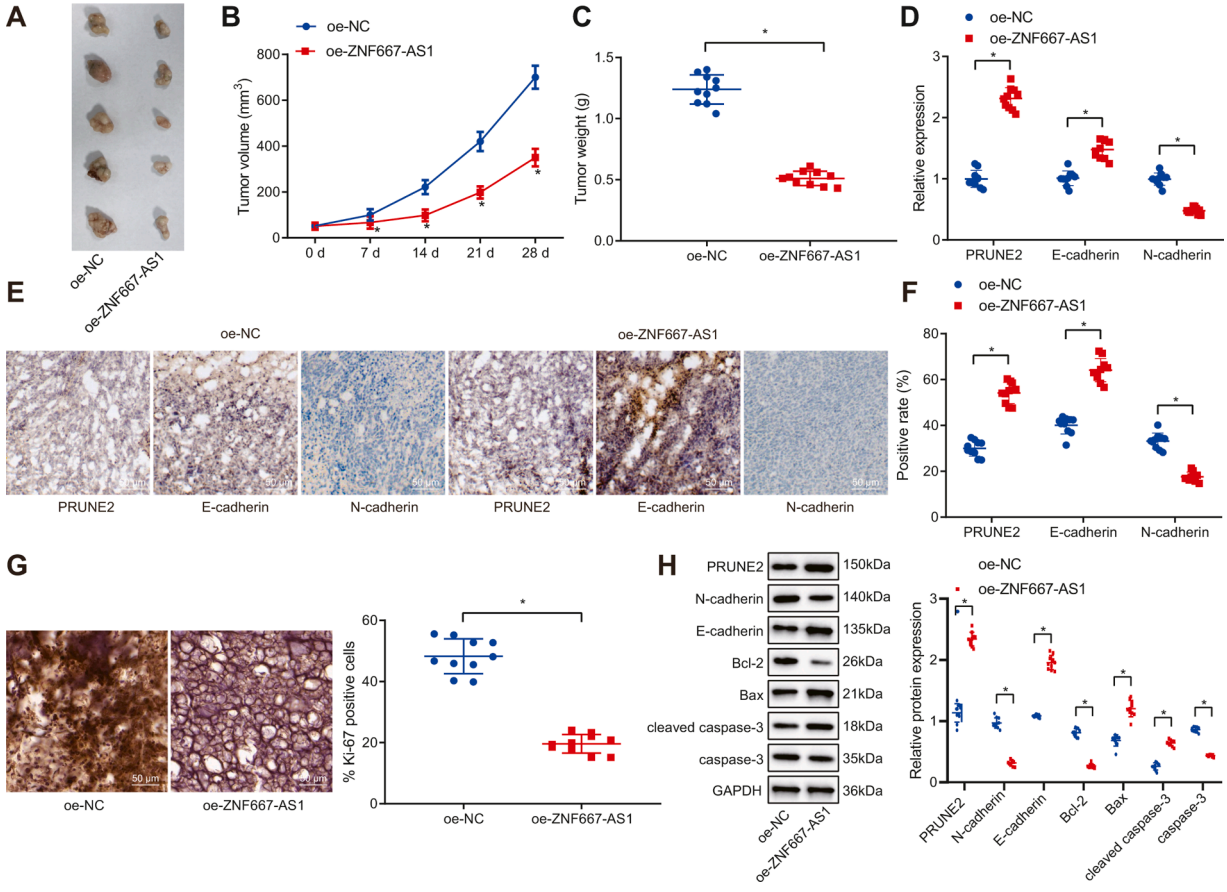

Fig. 6. ZNF667-AS1 inhibits the tumorigenesis of ESCC *in vivo*. The nude mice were subcutaneously injected with cells transfected with plasmids of oe-ZNF667-AS1. A, Representative images showing xenografts in nude mice. B, Tumor volume of nude mice within 4 weeks. C, Tumor weight of nude mice after 4 weeks of injection. D, mRNA expression of PRUNE2, E-cadherin and N-cadherin in the tumor tissues of mice measured by RT-qPCR. E, Representative images of immunohistochemistry analysis of PRUNE2, E-cadherin and N-cadherin proteins in the tumor tissues of mice (200 ×). F, Quantitative analysis of Panel E. G, Representative images of immunohistochemistry analysis of Ki-67 protein in the tumor tissues of mice (200 ×). H, Western blot analysis of PRUNE2, E-cadherin, N-cadherin, Bcl-2, Bax, cleaved caspase-3 and caspase-3 proteins in the tumor tissues of mice. * $p < 0.05$ *vs.* the mice treated with oe-NC. Statistical data are measurement data, and summarized as mean ± standard deviation. Comparison of data between two groups was conducted by unpaired *t*-test and that between multiple groups at different points using Bonferroni-corrected repeated measures ANOVA. $n = 10$.

and caspase-3 yet increases in that of E-cadherin, Bax and cleaved caspase-3 were observed in the presence of ZNF667-AS1 overexpression (Fig. 6H).

Discussion

ESCC is the most aggressive type of cancer among several gastrointestinal malignancies [24]. Despite recent rapid improvements in ESCC treatment, its prognosis remains unfavorable [25]. Identification and validation of sensitive and specific biomarkers for this cancer are thus of tremendous potential value. Alterations in specific lncRNAs have been identified in tumor cells and can serve as potential biomarkers for early cancer diagnosis or as potential drug targets [26]. In our current study, we demonstrated that ZNF667-AS1 played an inhibitory role in the development of ESCC by modulation of miR-1290-mediated PRUNE2.

One previous study noted a decline in ZNF667-AS1 expression in cervical cancer tissues and that ZNF667-AS1 was capable of limiting the proliferation of cervical cancer cells [9]. Additionally, decreased ZNF667-AS1 was also seen in laryngeal squamous cell carcinoma, specifically, overexpression of ZNF667-AS1 suppressed the malignant features of laryngeal squamous cell carcinoma cells [10]. In our study, we also discovered a decline in ZNF667-AS1 expression in both ESCC tissues and cell lines. Moreover, ZNF667-AS1 was negatively correlated with the occurrence and deterioration of ESCC since elevated ZNF667-AS1 reduced the malignant features of ESCC cells.

Accruing research reveals the correlation between aberrant expression of miR-1290 with the malignant process in several cancers. For instance, in colon cancer, elevated miR-1290 is detected, and decreasing its expression can induce cancer cell apoptosis [27]. Increased miR-1290 is also seen in non-small cell lung cancer cells and this increase in cancer cells can increase tumorigenesis [28], suggesting that miR-1290 impinges tumor initiation and progression. Furthermore, congruent with our findings, the overexpression of miR-1290 is found to promote the malignant characteristics of ESCC cells [27]. Our study also demonstrated a marked increase in miR-1290 in ESCC tissues and elevated miR-1290 could potentiate the malignant characteristics of ESCC cells.

Recently, multiple lncRNAs are capable of competing with mRNAs for binding to miRNAs and to lead to the development of disease [29]. According to the bioinformatics analysis performed in this study, binding sites were determined between ZNF667-AS1 and miR-1290, and ZNF667-AS1 was able to directly bind to miR-1290 in ESCC. LncRNA GAS5 could inhibit the growth of ESCC cells by competitively binding to miR-196a [30]. Another key observation in our study was that ZNF667-AS1 elevated PRUNE2 by binding to miR-1290, which ultimately curtailed the malignant potentials of ESCC cells. LncRNA-miRNA-mRNA interaction has been demonstrated in ESCC whereby lncRNAs regulate mRNA expression through interacting with miRNAs [31, 32]. Specifically, lncRNA PTENP1 overexpression in ESCC cells results in inhibited cell proliferation via binding to miR-17–5p and upregulating SOCS6 expression [33]. Increasing evidence shows that PRUNE2 is a functional target involved in tumor progression. PRUNE2 overexpression can decrease the proliferation of prostate cancer cells *in vitro* and suppresses tumor growth in tumor-bearing mice [15]. Besides, elevated PRUNE2 expression serves as a favorable prognostic factor for leiomyosarcoma patients [34]. PRUNE2 also functions as a tumor suppressor in oral cancer as its upregulation results in suppression of oral cancer migration [35]. Overall, current evidence indicates that ZNF667-AS1 can competitively bind to miR-1290 to suppress the malignant properties of ESCC cells by upregulating PRUNE2.

Conclusions

In conclusion, our study described a novel ZNF667-AS1/miR-1290/PRUNE2 regulatory axis in which ZNF667-AS1 downregulated miR-1290 by binding to miR-1290 and elevated PRUNE2 expression, thereby inhibiting ESCC (Fig. 7). Focus on lncRNA/miRNA/mRNA axis may summarize a better understanding for ESCC pathogenesis and accelerate the development of ceRNA-based therapy. In addition, we used multiple data sets to avoid the high false positive rate of a single data set analysis, but many data sets may cause inter-batch differences that cannot be avoided or eliminated. Moreover, it is unclear whether the use of background correction is reliable, because every data sets using different correction methods.

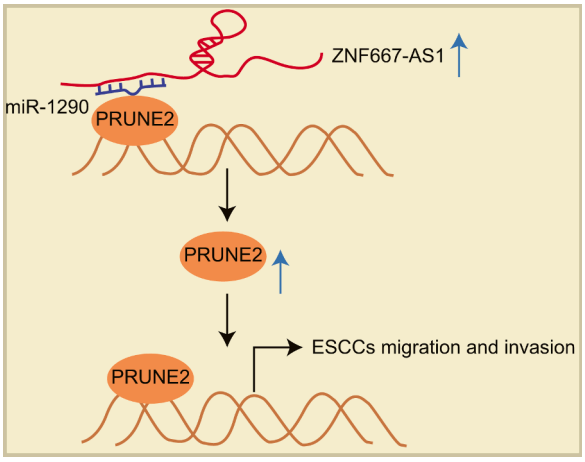

Fig. 7. The schematic diagram depicts the effect of ZNF667-AS1 and PRUNE2 on the development of ESCC. ZNF667-AS1 competitively binds to miR-1290 and up-regulates the expression of miR-1290 target gene PRUNE2, thus inhibiting the proliferation, migration and invasion of ESCC cells while inducing their apoptosis. ESCC progression is eventually arrested.

Supplementary Fig. 1 A heat map of the first 30 differentially expressed lncRNAs following analysis of the ESCC-related GSE45670 dataset. The abscissa represents the sample number, and the ordinate represents the differential expressed lncRNAs; the histogram at the upper right refers to color gradation; each rectangle corresponds to a sample expression value.

Funding

None.

Consent for publication

Not applicable.

Availability of data and material

The data that supports the findings of this study are available on request from the corresponding author.

CRediT authorship contribution statement

Ying-Juan Zheng: Conceptualization, Methodology, Project administration, Resources, Writing – original draft, Writing – review & editing. **Tian-Song Liang:** Conceptualization, Methodology, Project administration, Resources, Writing – original draft, Writing – review & editing. **Juan Wang:** Conceptualization, Data curation, Formal analysis. **Jing-Yi Zhao:** Conceptualization, Data curation, Formal analysis. **Su-Nan Zhai:** Conceptualization, Data curation, Formal analysis. **Dao-Ke Yang:** Conceptualization, Writing – original draft, Writing – review & editing. **Li-Dong Wang:** Conceptualization, Writing – original draft, Writing – review & editing.

Declaration of Competing Interest

The authors declare no conflicts of interest.

Acknowledgments

Not applicable.

Supplementary materials

Supplementary material associated with this article can be found, in the online version, at doi:10.1016/j.tranon.2022.101371.

References

[1] Z.W. Reichenbach, M.G. Murray, R. Saxena, D. Farkas, E.G. Karassik, A. Klochkova, et al., Clinical and translational advances in esophageal squamous cell carcinoma, Adv. Cancer. Res. 144 (2019) 95–135.
[2] H. Liang, J.H. Fan, Y.L. Qiao, Epidemiology, etiology, and prevention of esophageal squamous cell carcinoma in China, Cancer Biol. Med. 14 (1) (2017) 33–41.
[3] C.C. Abnet, M. Arnold, W.Q. Wei, Epidemiology of esophageal squamous cell carcinoma, Gastroenterology 154 (2) (2018) 360–373.
[4] Y.S. Tong, X.W. Wang, X.L. Zhou, Z.H. Liu, T.X. Yang, W.H. Shi, et al., Identification of the long non-coding RNA POU3F3 in plasma as a novel biomarker for diagnosis of esophageal squamous cell carcinoma, Mol. Cancer 14 (2015) 3.
[5] Y. Zhang, Y. Tao, Q. Liao, Long noncoding RNA: a crosslink in biological regulatory network, Brief. Bioinform. 19 (5) (2018) 930–945.
[6] J. Xu, J. Zhang, F. Shan, J. Wen, Y. Wang, SSTR5AS1 functions as a ceRNA to regulate CA2 by sponging miR15b5p for the development and prognosis of HBVrelated hepatocellular carcinoma, Mol. Med. Rep. 20 (6) (2019) 5021–5031.
[7] J. Fan, J. Zhang, S. Huang, P. Li, lncRNA OSER1-AS1 acts as a ceRNA to promote tumorigenesis in hepatocellular carcinoma by regulating miR-372-3p/Rab23 axis, Biochem. Biophys. Res. Commun. 521 (1) (2020) 196–203.
[8] L. Gou, H. Zou, B. Li, Long noncoding RNA MALAT1 knockdown inhibits progression of anaplastic thyroid carcinoma by regulating miR-200a-3p/FOXA1, Cancer Biol. Ther. 20 (11) (2019) 1355–1365.
[9] L.P. Zhao, R.H. Li, D.M. Han, X.Q. Zhang, G.X. Nian, M.X. Wu, et al., Independent prognostic factor of low-expressed LncRNA ZNF667-AS1 for cervical cancer and inhibitory function on the proliferation of cervical cancer, Eur. Rev. Med. Pharmacol. Sci. 21 (23) (2017) 5353–5360.
[10] W. Meng, W. Cui, L. Zhao, W. Chi, H. Cao, B. Wang, Aberrant methylation and downregulation of ZNF667-AS1 and ZNF667 promote the malignant progression of laryngeal squamous cell carcinoma, J. Biomed. Sci. 26 (1) (2019) 13.
[11] H. Xiao, K. Tang, P. Liu, K. Chen, J. Hu, J. Zeng, et al., LncRNA MALAT1 functions as a competing endogenous RNA to regulate ZEB2 expression by sponging miR-200s in clear cell kidney carcinoma, Oncotarget 6 (35) (2015) 38005–38015.
[12] J. Huang, M. Shen, M. Yan, Y. Cui, Z. Gao, X. Meng, Exosome-mediated transfer of miR-1290 promotes cell proliferation and invasion in gastric cancer via NKD1, Acta Biochim. Biophys. Sin. 51 (9) (2019) 900–907.
[13] H. Sun, L. Wang, Q. Zhao, J. Dai, Diagnostic and prognostic value of serum miRNA-1290 in human esophageal squamous cell carcinoma, Cancer Biomark. 25 (4) (2019) 381–387.
[14] E. Iwama, D. Tsuchimoto, T. Iyama, K. Sakumi, A. Nakagawara, K. Takayama, et al., Cancer-related PRUNE2 protein is associated with nucleotides and is highly expressed in mature nerve tissues, J. Mol. Neurosci. 44 (2) (2011) 103–114.
[15] A. Salameh, A.K. Lee, M. Cardo-Vila, D.N. Nunes, E. Efstathiou, F.I. Staquicini, et al., PRUNE2 is a human prostate cancer suppressor regulated by the intronic long noncoding RNA PCA3, Proc. Natl. Acad. Sci. USA 112 (27) (2015) 8403–8408.
[16] L. Gautier, L. Cope, B.M. Bolstad, R.A. Irizarry, affy–analysis of Affymetrix GeneChip data at the probe level, Bioinformatics 20 (3) (2004) 307–315.
[17] G.K. Smyth, Linear models and empirical bayes methods for assessing differential expression in microarray experiments, Stat. Appl. Genet. Mol. Biol. 3 (2004) Article3.
[18] D. Mas-Ponte, J. Carlevaro-Fita, E. Palumbo, T. Hermoso Pulido, R. Guigo, R. Johnson, LncATLAS database for subcellular localization of long noncoding RNAs, RNA 23 (7) (2017) 1080–1087.
[19] K.C. Miranda, T. Huynh, Y. Tay, Y.S. Ang, W.L. Tam, A.M. Thomson, et al., A pattern-based method for the identification of MicroRNA binding sites and their corresponding heteroduplexes, CellCell 126 (6) (2006) 1203–1217.
[20] X. Hu, D. Wu, X. He, H. Zhao, Z. He, J. Lin, et al., circGSK3beta promotes metastasis in esophageal squamous cell carcinoma by augmenting beta-catenin signaling, Mol. Cancer 18 (1) (2019) 160.
[21] L. Zhang, Y. Gao, X. Zhang, M. Guo, J. Yang, H. Cui, et al., TSTA3 facilitates esophageal squamous cell carcinoma progression through regulating fucosylation of LAMP2 and ERBB2, Theranostics 10 (24) (2020) 11339–11358.
[22] H. Wang, G. Sun, P. Xu, J. Lv, X. Zhang, L. Zhang, et al., Circular RNA TMEM87A promotes cell proliferation and metastasis of gastric cancer by elevating ULK1 via sponging miR-142-5p, J. Gastroenterol. 56 (2) (2021) 125–138.
[23] D. Milani, O.M. Palacios-Gimenez, D.C. Cabral-de-Mello, The U2 snDNA is a useful marker for B chromosome detection and frequency estimation in the grasshopper Abracris flavolineata, Cytogenet. Genome Res. 151 (1) (2017) 36–40.
[24] R. Liu, J. Gu, P. Jiang, Y. Zheng, X. Liu, X. Jiang, et al., DNMT1-microRNA126 epigenetic circuit contributes to esophageal squamous cell carcinoma growth via ADAM9-EGFR-AKT signaling, Clin. Cancer Res. 21 (4) (2015) 854–863.
[25] L. Hu, Y. Wu, D. Tan, H. Meng, K. Wang, Y. Bai, et al., Up-regulation of long noncoding RNA MALAT1 contributes to proliferation and metastasis in esophageal squamous cell carcinoma, J. Exp. Clin. Cancer Res. 34 (2015) 7.
[26] J. Li, H. Meng, Y. Bai, K. Wang, Regulation of lncRNA and Its Role in Cancer Metastasis, Oncol. Res. 23 (5) (2016) 205–217.
[27] L. Ye, T. Jiang, H. Shao, L. Zhong, Z. Wang, Y. Liu, et al., miR-1290 is a biomarker in DNA-mismatch-repair-deficient colon cancer and promotes resistance to 5-fluorouracil by directly targeting hMSH2, Mol. Ther. Nucleic Acids 7 (2017) 453–464.
[28] W.C. Zhang, T.M. Chin, H. Yang, M.E. Nga, D.P. Lunny, E.K. Lim, et al., Tumour-initiating cell-specific miR-1246 and miR-1290 expression converge to promote non-small cell lung cancer progression, Nat. Commun. 7 (2016) 11702.
[29] J.Y. Tan, T. Sirey, F. Honti, B. Graham, A. Piovesan, M. Merkenschlager, et al., Extensive microRNA-mediated crosstalk between lncRNAs and mRNAs in mouse embryonic stem cells, Genome Res. 25 (5) (2015) 655–666.
[30] K. Wang, J. Li, G. Xiong, G. He, X. Guan, K. Yang, et al., Negative regulation of lncRNA GAS5 by miR-196a inhibits esophageal squamous cell carcinoma growth, Biochem. Biophys. Res. Commun. 495 (1) (2018) 1151–1157.
[31] K. Ren, Y. Li, H. Lu, Z. Li, Z. Li, K. Wu, et al., Long Noncoding RNA HOTAIR controls cell cycle by functioning as a competing endogenous RNA in esophageal squamous cell carcinoma, Transl. Oncol. 9 (6) (2016) 489–497.
[32] C. Zhang, L. Wang, J. Yang, Y. Fu, H. Li, L. Xie, et al., MicroRNA-33a-5p suppresses esophageal squamous cell carcinoma progression via regulation of lncRNA DANCR and ZEB1, Eur. J. Pharmacol. 861 (2019), 172590.
[33] T. Gong, S. Zheng, S. Huang, S. Fu, X. Zhang, S. Pan, et al., PTENP1 inhibits the growth of esophageal squamous cell carcinoma by regulating SOCS6 expression and correlates with disease prognosis, Mol. Carcinog. 56 (12) (2017) 2610–2619.
[34] L.R. Zhao, W. Tian, G.W. Wang, K.X. Chen, J.L. Yang, The prognostic role of PRUNE2 in leiomyosarcoma, Chin. J. Cancer 32 (12) (2013) 648–652.
[35] S.C. Su, C.M. Yeh, C.W. Lin, Y.H. Hsieh, C.Y. Chuang, C.H. Tang, et al., A novel melatonin-regulated lncRNA suppresses TPA-induced oral cancer cell motility through replenishing PRUNE2 expression, J. Pineal Res. 71 (3) (2021) e12760.